 doi:10.20944/preprints202008.0162.v1

Article

Efficiency of selective solar absorber in high vacuum flat solar thermal panels: The role of emissivity and cut-off wavelength

Davide De Maio [1,2], Carmine D'Alessandro [1,2], Antonio Caldarelli [1,2], Marilena Musto [1], Daniela De Luca [3,2], Emiliano Di Gennaro [3] and Roberto Russo [2]

[1] Industrial Engineering Department, University of Napoli "Federico II", Napoli, Italy;
[2] Istituto di Scienze Applicate e Sistemi Intelligenti, Unità di Napoli;
[3] Physics Department, University of Napoli "Federico II", Napoli, Italy;
* Correspondence: Davide.demaio@na.isasi.cnr.it ;

Abstract: A multilayer structure on a metallic substrate has been optically simulated and the optimization procedure aimed at obtaining Selective Solar Absorber (SSA) is discussed. This study refers to flat high vacuum thermal collectors and the overall Sun-to-thermal conversion efficiency has been evaluated using analytical formula and numerical thermal model. Both methods are in agreement and they have been validated using experimental results on a commercial absorber. The importance of a low emittance value to obtain high thermal efficiency at high temperatures and high stagnation temperature in selective solar absorber is highlighted. Optimized absorbers can be 8% more efficient than the commercial alternative at 250 °C operating temperatures and up to 27% more efficient at 300 °C. A stagnation temperature higher than 400 °C can be reached without Sun concentration if the proper design is adopted.

Keywords: Thermal emittance; conversion efficiency; selective solar absorber; thermal energy; evacuated flat panel; solar energy

1. Introduction

Solar energy will play a key role in the energy transition from fossil fuels to renewable energy [1–5]. More than one fourth of the energy resources in the developed countries is nowadays used for heating and cooling [6–8]. Such large fraction of energy can be provided by Solar thermal collectors converting solar energy directly into heat with high efficiency and significantly reducing the carbon footprint of industrialized countries. The core component in a solar thermal collector is the Selective Solar Absorber (SSA). The idea was first introduced at the end of '50, and since then, several works have been devoted to study and to optimize SSA [9–22]. The ideal SSA should efficiently absorb solar radiation (solar absorptance α=1), whereas its thermal emission should be minimal (emissivity ϵ=0). Its spectral emissivity is assumed to be a step function from 1 to 0 [11,23,24] and the wavelength where the transition happens is commonly named cut-off wavelength ($\lambda_{cut\text{-}off}$) [23,24]. The formal definition of $\lambda_{cut\text{-}off}$ leads to energetic considerations: it is chosen in order to maximize the absorber thermal performance and it depends on the working temperature and on solar incoming power (i.e. solar concentration ratio) [10,23]. It is verified that $\lambda_{cut\text{-}off}$ is the wavelength at which the blackbody emission curve crosses the solar radiation spectrum [10,24].

In Fig. 1a we report the solar spectrum with the blackbody emission together with the ideal emissivity curve calculated for 100 °C and 300 °C of absorber working temperature without concentration.

At low temperature, blackbody emission and solar spectrum barely overlap and the optimization of the SSA limits to maximize the solar absorption, since the demanded emissivity transition (from high absorptance in solar range and low emission in black body emission spectrum) is easy to obtain in

 doi:10.20944/preprints202008.0162.v1

a wide wavelength range. Several absorbers are commercially available [25,26] and they are designed to operate in flat collectors at temperature below 100 °C.

When the operating temperature increases over 200 °C, the blackbody emission starts to overlap the solar spectrum. Due to the zero intensity of solar irradiation on Earth in some peculiar wavelengths (as in the range 1.8-2.2 μm) the optimal $\lambda_{\text{cut-off}}$ presents some "hidden regions" that are usually excluded from the optimization [10]. In order to investigate such aspect, some authors studied the impact of a not perfect emissivity of the ideal SSA (absorptance values lower than 1 below the $\lambda_{\text{cut-off}}$ and higher than 0 above) and they stated that the ideal cut-off wavelength does not depend on the adopted emissivity [10,27].

Recently Yang et al.[18] have studied the effect of non-ideal SSA properties on the overall performances in a Concentrated Solar Power (CSP) system: their theoretical SSA has a finite slope in the cut-off transition (instead of the ideal step function) and not ideal SSA emissivity. The optimal cut-off wavelengths also showed some "hidden regions" slightly shifted respect to the ideal SSA, due to their different definition for cut-off wavelength.

To design a solar selective coating, various architectures are available: they include intrinsic absorber, semiconductor-metal tandem, dielectric-metal multilayer, cermet, surface texturing, and photonic crystal. They have been periodically summarized in review papers [10,11,23,24,27,28]. Also very recent works developing new idea in SSA such as 3D structured graphene [21], multi-layered cermet [13], nanomultilayer [29] or high entropy alloy [9] use $\lambda_{\text{cut-off}}$ as defined in [10].

Dealing with a real SSA, the relative importance of solar absorptance and thermal emittance to calculate the absorber efficiency has to be taken in to account. Cao introduced a Weighting Factor (w) as defined in [10] that indicates the relative weight of α and ϵ(T) in the efficiency of a solar absorber. In Fig. 1b the Weighting factor is reported as a function of the absorber temperature and solar concentration. All selective absorbers, in literature as in commerce, have been optimized for concentrated collectors or flat plate collectors without vacuum insulation, conditions with w much lower than 1.

The importance of vacuum insulation in solar thermal panel has been already highlighted [30], however only recently TVP Solar [31] presented a new High Vacuum insulated Flat plate solar thermal Panel (HVFP) [32]. High vacuum insulation reduces the internal gas convective and conductive losses to a negligible level, keeping high conversion efficiency at high working temperature. The increased panel efficiency due to high vacuum has been studied also from other researchers [33,34]. In HVFP the thermal radiation is the main loss mechanism and the radiative properties of SSA are an aspect of primary importance. It is worth to note that thermal emittance gains importance over the absorptance as the working temperature increases (green arrow in Fig. 1b) and that HVFPs represent the only commercial product with w higher than 1.

At present HVFPs include the absorber Mirotherm® from Alanod, a commercial SSA optimized for low working temperatures (up to about 150 °C). It results in excellent performance up to 180 °C , however at higher temperatures the low selectivity of the absorber increases the thermal radiation losses, affecting panel efficiency and limiting the stagnation temperature at about 320°C with an illumination of 1000 W/m^2. In this work a multilayer absorber consisting of Cr_2O_3/Ti/Cr_2O_3 on smooth Aluminium substrate has been numerically investigated. Multilayer absorbers allow to control thermal emission while guaranteeing high solar absorption, excellent thermal stability and their optical properties can be easily simulated [9,12,14,20,35,36].

A single SiO_2 layer has been used as antireflective coating to improve absorptance. The simulated emissivity curves are used to evaluate the temperature dependent spectrally averaged emissivity which in turn allows to evaluate the radiative losses and the SSA efficiency. The efficiency of the new absorber is discussed in comparison with the efficiency of commercially available absorber actually used in HVFPs, taking in to account the non-ideal cut-off in the emissivity curve of both SSA.

Preprints (www.preprints.org) | NOT PEER-REVIEWED | Posted: 6 August 2020 doi:10.20944/preprints202008.0162.v1

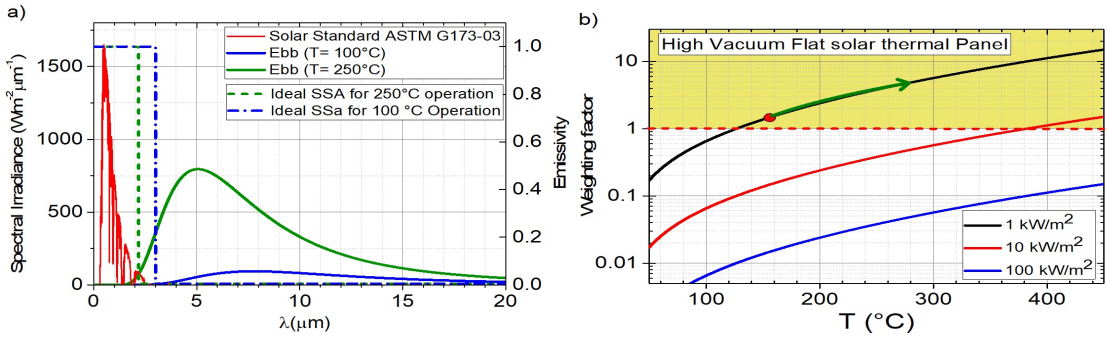

Figure 1. (a) left axis: Blackbody emission E_{bb} (left axis) for 100 °C working temperature (blue line) and 300 °C working temperature (green line) vs Solar Spectrum (red line); right axis: Ideal spectral emissivity for Selective Solar Absorber working at 100 °C (blue dashed line) and 300 °C (green dashed line) (b) Weighting factor versus Absorber temperature T_h (°C) for different solar concentration ratios. The red dot indicates the operating temperature (150 °C) and the green arrow the increasing importance of thermal emittance with working temperature (adapted from [10]).

2. Numerical analysis: coating design and optimization

Multilayer absorbers consist in stacks of alternating dielectric layers (high absorptance in visible range, transparent in Infrared region) and metal absorption layers (thin enough to allow for partial transparency). Absorption is guaranteed by multiple reflections at interfaces, while spectrally averaged emissivity is mainly due to the low-emissive metal substrate (IR reflector) [12,19,35,36]. In this study a tri-layered structure has been investigated. A Titanium absorbing layer is sandwiched between two Chromium Oxide (Cr_2O_3) dielectric layers on an Aluminium substrate acting as IR reflector. Al_2O_3 natural passivation layer of the Al substrate has been included in the numerical simulations model. The multilayer structure is completed by an antireflective coating (ARC) based on SiO_2 to further enhance solar absorption.

IMD software is used for numerical simulations [37]. The materials constituting the solar absorber were deposited by e-beam evaporation and their complex refractive index were experimentally estimated in a previous work [17].

A genetic algorithm is used to adjust layer thicknesses in order to fit a target curve [37]. The genetic algorithm creates a starting population of individuals (in our case multilayers with different layer thicknesses) and a Figure of Merit (FOM) is determined; only individuals with best FOM will be retained. FOM function is written as follows 1:

$$FOM = \frac{\sum_{i=1}^{N_{mo}} w[i] \cdot |Y[i] - Y_{mo}[i]|^n}{\sum_{i=1}^{N_{mo}} w[i]} \quad (1)$$

where w[i] is the weighting factor for the i-point, Y[i] is the value of the function being optimized for the i-point, Y_{mo}[i] is the value of the target function for the i-point. $\Delta(FOM)/FOM < \zeta$ (with ζ the convergence tolerance value) determines the convergence of the algorithm. Δ(FOM)=<FOM>-FOM and the quantity <FOM> corresponds to the average of FOM over the previous X generations of individuals. The n exponent is used to compute the FOM itself and needs to be specified.

As a target function we used the spectral emissivity curve of an ideal selective solar absorber with cut-off wavelengths obtained for different temperatures.

3. Results and discussion

The optimization procedure described in the previous section has been repeated for the various target cut-off wavelengths obtained for different working temperature from 200 °C up to 350 °C. Fig. 2a shows the spectral emissivity for 4 different multilayer absorbers obtained as the result of the optimization process (200 °C, 250 °C, 300 °C, 350 °C; cyan, black, green, blue and red solid lines, respectively). Table 1 sums up the $\lambda_{cut\text{-}off}$ values, layer thickness, solar absorptance α_S, and thermal

Preprints (www.preprints.org) | NOT PEER-REVIEWED | Posted: 6 August 2020 doi:10.20944/preprints202008.0162.v1

emittance ϵ_T at 200 °C, 250 °C, 300 °C and 350 °C for each selective coating. Solar absorptance and temperature dependent emittance (also referred as spectrally averaged emissivity) are calculated from the spectral emissivity curves as in the following equations 2 and 3:

$$\alpha_S = \frac{\int \epsilon(\lambda) \cdot S_{SUN}(\lambda)\, d\lambda}{\int S_{SUN}(\lambda)\, d\lambda} \tag{2}$$

$$\epsilon_T = \frac{\int \epsilon(\lambda) \cdot E_{bb}(\lambda, T)\, d\lambda}{\int E_{bb}(\lambda, T)\, d\lambda} \tag{3}$$

with S_{Sun} and E_{bb} being the solar spectral irradiance and the blackbody radiation, respectively and the integral is calculated in the wavelength regions where S_{Sun} (λ) and E_{bb} (λ,T) are different from zero.

Table 1. Operating temperature, $\lambda_{cut\text{-}off}$ for desired operating temperature, layer thickness obtained from the optimization process, solar absorptance α_S and thermal emittance ϵ_T at 200 °C, 250 °C, 300 °C and 350 °C calculated from eq. 2 and 3, for 5 simulated multilayer absorbers and a commercial absorber.

SSA name	A	B	C	D	E
Operating Temperature (°C)	200	250	300	350	-
$\lambda_{cut\text{-}off\ CAO}$ (μm)	2.47	2.37	2.19	1.79	1.5
Top dielectric layer thickness (nm)	110	98	81	59	46
Metal layer thickness (nm)	16	16	15	13	12
Bottom dielectric layer thickness (nm)	42	38	32	25	20
Anti-Reflective Coating	70	67	63	60	52
Solar absorptance α_S	0.91	0.91	0.91	0.89	0.86
Thermal Emittance ϵ_T (200 °C)	0.056	0.050	0.041	0.031	0.026
Thermal Emittance ϵ_T (250 °C)	0.067	0.060	0.048	0.035	0.029
Thermal Emittance ϵ_T (300 °C)	0.080	0.071	0.057	0.041	0.034
Thermal Emittance ϵ_T (350 °C)	0.094	0.083	0.066	0.047	0.038

The results of the optimization process show that the cut-off wavelength of the selective solar absorber can be adjusted by varying the layer thicknesses, preserving a high solar absorption and a low thermal emission. The ideal cut off intercepts the emissivity curve at about 0.5 for all temperatures. In Fig. 2b, temperature dependent emittance of multilayers, calculated according to eq.3, is compared with the commercial coating currently used in high-vacuum solar collectors (dashed line). Multilayer with lower cut-off wavelengths can reduce the room temperature emittance and, more important, its temperature dependence resulting in a more than 50% emittance reduction at all temperature values. We will see that the emissivity reduction will result in an increased efficiency.

Preprints (www.preprints.org) | NOT PEER-REVIEWED | Posted: 6 August 2020 doi:10.20944/preprints202008.0162.v1

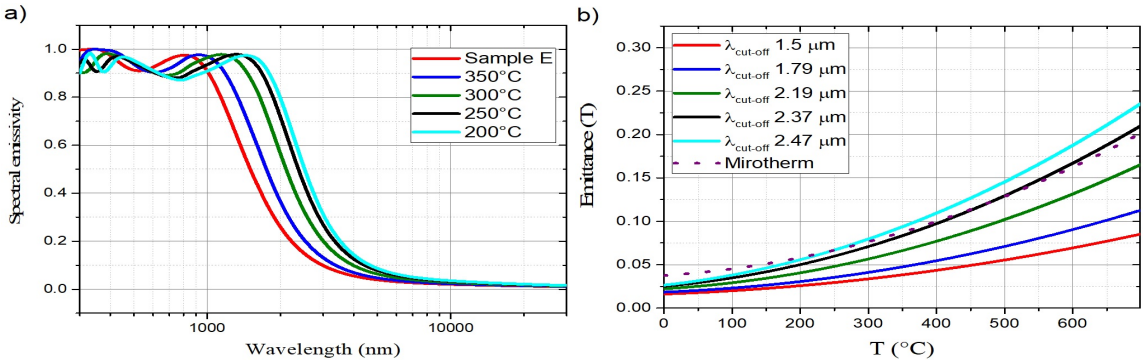

Figure 2. (a) Spectral emissivity of multilayer selective absorbers optimized for different temperature and consequent cut-off wavelength. (b) Temperature dependent emittance for different cut-off wavelength calculated using eq.3.

The SSA efficiency can be written as following:

$$\eta_{\text{Selective coating}} = \frac{q_h}{H_{abs}} = \alpha_s - \frac{\epsilon(T_h) \cdot \sigma_{SB}({T_h}^4 - {T_{amb}}^4)}{H_{abs}} \quad (4)$$

where $\eta_{\text{selective coating}}$ = Coating efficiency, α_S = Solar absorptance, $\epsilon(T_h)$ = Temperature dependent thermal emittance, q_h = Heat flux to the thermal system (Wm^{-2}), H_{abs} = Solar Irradiance on the absorber (Wm^{-2}), T_h = Absorber temperature (K), T_{amb} = Temperature of the environment (K), σ_{SB} = Stefan-Boltzmann constant ($Wm^{-2}K^{-4}$).

The SSA efficiency for the simulated multilayers and the commercial absorber, calculated from equation 4, is plotted in Fig. 3. The graph shows how temperature dependent emittance shapes the selective absorber performance curves. Mirotherm® commercial absorber is optimized for standard flat-plate solar collectors. It shows the highest efficiency for lower values of operating temperature because of its higher solar absorption coefficient and a relatively low spectrally averaged emissivity, at low working temperatures (see Fig.2b). Multilayers A and B are good options for mid temperature applications: although these two coatings have a lower solar absorptance α_S with respect to the commercial absorber, the improvement in thermal emittance (Fig. 2b, table 1) results comparable performances for high working temperatures. Multilayer C and D offers the highest stagnation temperatures thanks to the lowest spectrally averaged emissivity, but a slightly lower efficiency in low to mid temperatures range, due to low cut off that reduces the power available from the Sun spectrum, resulting in a low absorptance. However, starting from 200 °C they present a coating efficiency higher than the other absorbers, including the Mirotherm®.

It is worth to note that cut-off values, obtained and reported in table 1, are very close to the edge of the regions 1.6-1.8 μm and 2.2-2.5 μm, that are usually investigated [10]. In Fig.3 we report also efficiency calculated using an emissivity curve obtained with a 1.5 μm cut-off which is outside the typically explored wavelength interval, since it corresponds to a region of zero intensity in the Sun spectrum. It results in an efficiency higher than the efficiency obtained with the ideal cut off for all temperature above 300 °C. Such effect is the consequence of two factors: a) the optimization code is unable to obtain an emissivity curve close enough to the ideal curve and we deal with real absorber with α_S and ϵ_T defined by eqs. 2 and 3; b) at temperature higher that 300 °C the thermal radiation plays a major role determining the coating efficiency as indicated in Fig. 1b). In particular, the non-ideal behaviour of the emissivity curve means that real emittance (and absorptance) has to be taken in to account when calculating efficiency.

Preprints (www.preprints.org) | NOT PEER-REVIEWED | Posted: 6 August 2020 doi:10.20944/preprints202008.0162.v1

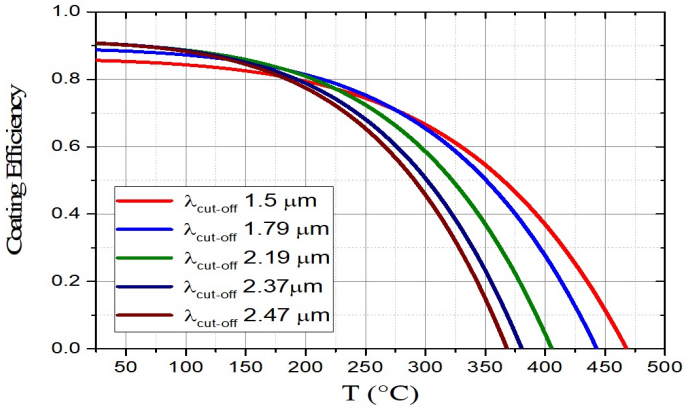

Figure 3. Absorber efficiency versus operating temperature for five multilayer absorbers with different cut-off wavelength (optimized for different temperatures), and Mirotherm® commercial absorber (blue dotted line).

A further reduction in $\lambda_{\text{cut-off}}$ below 1.5 μm can produce some increase of the stagnation temperature, however the Sun spectrum rises very fast when wavelength reduce below 1.4 μm and the reduction in absorptance drastically reduce the efficiency at lower temperatures (the curves are not reported here).

Eq. 4 allows to evaluate the coating efficiency without taking into account boundary conditions (such as the glass optical losses, conductive losses and substrate radiative losses due to the heat exchange between the back side of the absorber and the collector vessel). In case of negligible conductive and convective losses as the case of an absorber suspended in high vacuum, equation 4 can be modified in order to evaluate the *overall absorber efficiency*, $\eta_{overall\ abs}$ of a flat absorber as following:

$$\eta_{\text{overall abs}} = \tau_{\text{Glass}} \cdot \alpha_{\text{S}} - \frac{\epsilon(T_{\text{h}}) \cdot \sigma_{\text{SB}}({T_{\text{h}}}^4 - {T_{\text{amb}}}^4)}{H_{\text{abs}}} - \frac{\epsilon_{\text{Sub}} \cdot \sigma_{\text{SB}}({T_{\text{h}}}^4 - {T_{\text{amb}}}^4)}{H_{\text{abs}}} \tag{5}$$

where, τ_{Glass} is the glass transmittance and ϵ_{Sub} is the equivalent emissivity relative to the absorber back side and the vessel and it is assumed to be temperature independent. For Mirotherm®, a previous work [22] has shown that ϵ_{Sub}=0.045 provides an excellent fit to experimental data; it is in agreement with the spectrally averaged emissivity calculate by FTIR measurement. We can validate eq. 5 using an experimental setup [22,38] which allows to evaluate the overall efficiency of the absorber by performing stagnation temperature measurements in high vacuum. The experimental set-up, named Mini-Test-Box (MTB), consists of a stainless steel high-vacuum chamber, closed in the upper side by an extra-clear float glass, which can host a flat absorber suspended by four springs of negligible thermal conductivity. The MTB has been numerically simulated using Comsol Multiphysics [37]. The experimental data were obtained illuminating the absorber with different light power using a calibrated LED illumination system described in [39] and recording the absorber stagnation temperature [38]. In such configuration the power losses are equal to absorbed power $\epsilon(\text{T}_h)\cdot\sigma_{\text{SB}}\ (\text{T}_h^4 - T_{amb}^4)+\epsilon_{Sub}\cdot\sigma_{SB}(T_h^4 - T_{amb}^4) = \tau_{Glass}\alpha_{LED}P_{LED}$ and efficiency can be calculated, as reported below:

$$\eta(T_{\text{Abs}}) = \tau_{\text{glass}} \cdot \alpha_{\text{LED}} - \frac{\tau_{\text{glass}} \cdot \alpha_{\text{LED}} P_{\text{LED}}}{P_{\text{inc}}} \tag{6}$$

where P_{inc} is Sun irradiated power set to 1000 Wm^{-2}, τ_{glass} = 0.91 is the glass transmittance, α_{LED} = 0.95 is the absorptance α evaluated as in eq. 2, where the solar spectrum is replaced by the spectrum of the LED lump used to illuminate the absorber [39], P_{LED} is the light power provided by the calibrated LED system and Tabs is the stagnation temperature at a given LED power.

Fig. 4a reports the Mirotherm® overall efficiency (as from eq. 5) when placed in the Mini-Test-Box (blue solid line), the numerical simulation of the experimental setup (red dash-dot line) and the experimentally measured overall efficiency (black dots). The good agreement between numerical

Preprints (www.preprints.org) | NOT PEER-REVIEWED | Posted: 6 August 2020 doi:10.20944/preprints202008.0162.v1

simulations, measured data obtained by eq. 6 and values descending from eq. 5 confirms that, if the conductive losses are negligible and the proper ϵ_{Sub} is taken in to account, the eq. 5 is a valid instrument to evaluate the overall absorber efficiency.
Fig. 4b shows the overall efficiency calculated from equation 5 for the coating with different cut-off and an equivalent emittance of aluminium substrate of 0.045. The equivalent substrate emissivity is assumed to be constant with temperature.

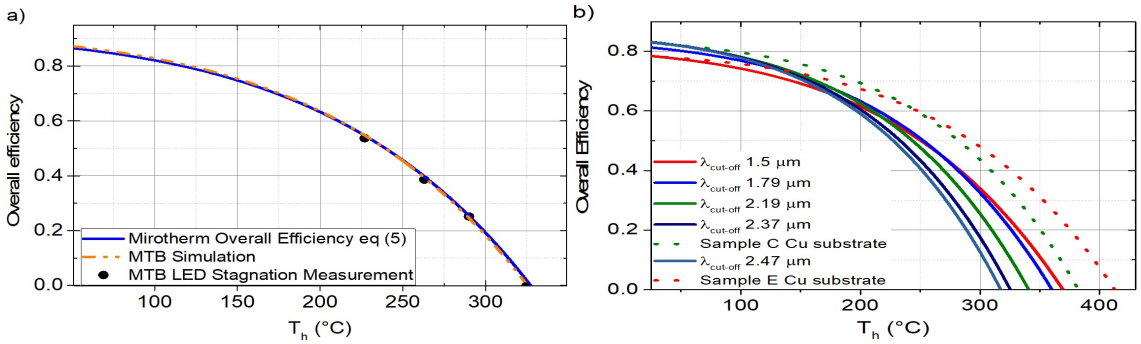

Figure 4. (a) Overall efficiency versus Absorber temperature T_h: Mini-test-box(MTB) simulated efficiency (red, dash dot), Led Measured MTB efficiency (black dots), Mirotherm® overall efficiency calculated using eq. 5 (blue solid line). (b) Overall efficiency calculated using eq. 5 for coating having different cut-off on aluminium substrate (solid lines) and for coatings with 2.0 μm and 1.5 μm cut-off deposited on copper substrate with ϵ(T)=0.02 (olive and red dashed line).

It can be noted that, reducing the cut-off, it does not influence dramatically the efficiency at low temperature; all efficiency values being around 0.8 except for 1.5 μm cut-off, because the too short cut-off wavelength causes a part of the solar spectrum to be outside of the high absorptance range. However, once the temperature increases the low emissivity plays a major role in preserving efficiency and at temperature higher than 300 °C the E coating performs better than all the others. It should be noted that for coating with cut-off lower than 2 μm, the coating emittance is lower than the industrial aluminium substrate emittance and a substrate with a lower emissivity can significantly improve efficiency. This result is not surprising: looking at the commercial absorber it is clear that the uncoated side of the absorber has a relative high roughness (Ra = 1.65 μm) and emissivity increases with roughness. On the other hand, the commercial absorbers have been developed for standard flat panel, where the uncoated side is insulated by rock wool, the coated side is in air or under inert atmosphere and it makes no sense to provide a better finishing to reduce aluminium emissivity.

Therefore, once a proper selective coating minimizes the thermal emittance of the solar absorber, the absorber overall efficiency can be significantly increased by the use of a very low emittance surface also on the uncoated side. Typical emissivity values for electropolished copper is 0.02 [40,41] whereas Silver films have been reported having an emissivity as low as 0.01 [42]. Eq. 6 has been calculated also for an equivalent substrate emissivity of 0.02. Results are reported in Fig. 4b as Olive (2.0 μm cut-off) and red (1.5 μm cut-off) dashed line, showing the importance of the uncoated side thermal properties to reach high temperatures with high efficiencies. In particular, choosing the proper cut-off and the proper substrate it is possible to achieve absorber efficiency higher than 50% at temperature up to 280 °C or a stagnation temperature in excess of 400 °C. In particular, at 300 °C the overall efficiency increase from 20% of Mirotherm to 44 and 48% with optimized coating on copper with a relative increase more than 100%.

4. Conclusion

We have numerically simulated a selective solar absorber for mid-temperature application based on Cr_2O_3 /Ti/Cr_2O_3 tri-layer on metallic substrate. As a target curve for the optimization process, at first we used the spectral emissivity curve of an ideal selective solar absorber with ideal cut-off

 doi:10.20944/preprints202008.0162.v1

wavelength, obtained for different working temperatures according to [10]. The optimization process results in solar selective coatings which offer remarkable advantages in terms of thermal emission with respect to a commercial absorber, currently used in high vacuum collectors, preserving high solar absorption (about 90%). We evaluated the efficiency of the absorber coating and the whole absorber using eqs. 5 and 6. The model has been validated measuring a commercial absorber (Mirotherm® from Alanod) and used to evaluate the performance of simulated multilayers. The absorber efficiency has been evaluated also for absorbers with emissivity curves obtained using as target curve an ideal absorber with cut-off wavelengths shorter than the ideal one and situated outside of the standard recommended region, defined according to [10]. Such absorbers have produced, at high temperatures, efficiency higher than the one obtained by absorber with ideal cut-off.

Our results show that a reduction in spectrally averaged emissivity is essential to reach high operating and/or high stagnation temperatures. Once the emissivity of the selective absorber has been optimized, the overall absorber performances can be further improved using a very low emittance material such as copper (or silver) on the absorber back side, allowing to reach operating temperature up to 300 °C, with overall coating efficiency of 48% with a 140% improvement respect to the commercial coating. The stagnation temperature can also be increased from 320 °C to more than 400 °C without concentration. Such performance will allow to HVFP to contribute to the energy transition from fossil fuels to renewable energy for efficient heat production.

References

1. Meinshausen, M., Meinshausen, N., Hare, W., Raper, S. C. B., Frieler, K., Knutti, R., Frame, D. J., Allen, M. R., Greenhouse-gas emission targets for limiting global warming to 2 °C. *Nature* **2009**, *458*, 1158–1162.
2. Lauterbach, C., Schmitt, B., Jordan, U., Vajen, K., The potential of solar heat for industrial processes in Germany. *Renewable and Sustainable Energy Reviews* **2012**, *16*, 5121–5130.
3. Shahsavari A., Morteza Akbari, Potential of solar energy in developing countries for reducing energy-related emissions. *Renewable and Sustainable Energy Reviews* **2018**, *90*, 275–291.
4. Rabia Akram, Fuzhong Chen, Fahad Khalid, Zhiwei Ye, Muhammad Tariq Majeed, Heterogeneous effects of energy efficiency and renewable energy on carbon emissions: Evidence from developing countries. *Journal of Cleaner Production* **2020**, *247*, 119–122.
5. Andrew J. Chapmana, Benjamin C. McLellan, Tetsuo Tezuka, Prioritizing mitigation efforts considering co-benefits, equity and energy justice: Fossil fuel to renewable energy transition pathways. *Applied Energy* **2018**, *219*, 187–198.
6. Tobias Fleiter, Rainer Elsland, Matthias Rehfeldt, Jan Steinbach, Ulrich Reiter, Giacomo Catenazzi, Martin Jakob, Cathelijne Rutten, Robert Harmsen, Florian Dittmann, Philippe Rivière, Pascal Stabat, Profile of heating and cooling demand in 2015.**2017**
7. Lukas Kranzl, Michael Hartner, Andreas Müller, Gustav Resch, Sara Fritz, Tobias Fleiter, Andrea Herbst, Matthias Rehfeldt, Pia Manz, Alyona Zubaryeva, Jonatan GÓMEZ VILCHEZ , Heating Cooling outlook until 2050, EU-28. **2018**.
8. Tobias Fleiter, Jan Steinbach, Mario Ragwitz, Marlene Arens, Ali Aydemir, Rainer Elsland, Clemens Frassine, Andrea Herbst, Simon Hirzel, Michael Krail, Matthias Rehfeldt, Matthias Reuter, Jörg Dengler, Benjamin Köhler, Arnulf Dinkel, Paolo Bonato, Nauman Azam, Doreen Kalz Heidenhofstr, Felipe Andres Toro, Christian Gollmer, Felix Reitze, Michael Schön, Eberhard Jochem, Frédéric Tuillé, GaëtanFovez, Diane Lescot, Michael Hartner, Lukas Kranzl, Andreas Müller, Sebastian Fothuber, Albert Hiesl, Marcus Hummel, Gustav Resch, Eric Aichinger, Sara Fritz, Lukas Liebmann, Agnė Toleikytė, Ulrich Reiter, Giacomo Catenazzi, Martin Jakob, Claudio Naegeli, Mapping and analyses of the current and future (2020 – 2030) heating/cooling fuel deployment (fossil/renewables). **2016**.
9. Guo, H.-X., He, C.-Y., Qiu, X.-L., Shen, Y.-Q., Liu, G., Gao, X.-H., A novel multilayer high temperature colored solar absorber coating based on high-entropy alloy MoNbHfZrTi: Optimized preparation and chromaticity investigation. *Solar Energy Materials and Solar Cells* **2020**, *209*.
10. Cao, F., McEnaney, K., Chen, G., Ren, Z., A review of cermet-based spectrally selective solar absorbers. *Energy Environmental Science* **2014**, *7*.

11. Xu, K., Du, M., Hao, L., Mi, J., Yu, Q., Li, S., A review of high-temperature selective absorbing coatings for solar thermal applications. *Journal of Materiomics* **2020**, *6*, 167–182.
12. A.B. Khelifa, S. Khamlich, Z.Y. Nuru, L. Kotsedi, A. Mebrahtu, M. Balgouthi, A.A. Guizani, W. Dimassi, M. Maaza, Growth and characterization of spectrally selective Cr2O3/Cr/Cr2O3 multilayered solar absorber by e-beam evaporation. *Journal of Alloys and Compounds* **2018**, *734*, 204–209.
13. Yuping Ning, Jian Wang, Chunhui Ou, Changzheng Sun, Zhibiao Hao, Bing Xiong, Lai Wang, Yanjun Han, Hongtao Li, Yi Luo , NiCr–MgF2 spectrally selective solar absorber with ultra-high solar absorptance and low thermal emittance. *Solar Energy Materials and Solar Cells* **2020**, *206*.
14. Xiao-Li Qiu, Xiang-Hu Gao, Cheng-Yu He, Gang Liu , Optical design, thermal shock resistance and failure mechanism of a novel multilayer spectrally selective absorber coating based on HfB2 and ZrB2. *Solar Energy Materials and Solar Cells* **2020**, *211*.
15. Atchuta, S. R., Sakthivel, S., Barshilia, H. C., Selective properties of high-temperature stable spinel absorber coatings for concentrated solar thermal application. *Solar Energy* **2020**, *199*, 453–459.
16. Wei Wang, Huaixing Wen, Xi Huan, Jing Shi, Zhengtong Li, Jinbu Su, Chengbing Wang, Single layer WOx films for efficient solar selective absorber. *Materials and Design* **2020**, *186*.
17. D'Alessandro, C., de Maio, D., de Luca, D., di Gennaro, E., Gioffrè, M., Iodice, M., Musto, M., Rotondo, G., Dalena, D., Russo, R. , Solar Selective Coating for Thermal Applications. *Key Engineering Materials* **2019**, *813*, 316–321.
18. Honglun Yang, Qiliang Wang, Yihang Huang, Junsheng Feng, Xianze Ao, Maobin Hu, Gang Pei , Spectral optimization of solar selective absorbing coating for parabolic trough receiver. *Energy* **2019**, *183*, 639–650.
19. T.K. Tsai, Y.H. Li, J.S. Fang , Spectral properties and thermal stability of CrN/CrON/Al2O3 spectrally selective coating. *Thin Solid Films* **2016**, *615*, 91–96.
20. N. Khoza, Z.Y. Nuru, J. Sackey, L. Kotsedi, N. Matinise, C. Ndlangamandla, M. Maaza, Structural and optical properties of ZrOx/Zr/ZrOx/AlxOy multilayered coatings as selective solar absorbers. *Journal of Alloys and Compounds* **2019**, *773*, 975–979.
21. Keng-Te Lin, Han Lin, Tieshan Yang, Baohua Jia, Structured graphene metamaterial selective absorbers for high efficiency and omnidirectional solar thermal energy conversion. *Nature Communications* **2020**, *11*.
22. R. Russo, M. Monti, C. D'Alessandro, D. De Maio, M. Musto, C. Koral, A. Andreone, F. Di Giamberardino, V.G. Palmieri, The Absorptance of Selective Solar Absorber Working in High Vacuum. *20th Italian National Conference on Photonic Technologies* **2018**.
23. Bermel, P., Lee, J., Joannopoulos, J. D., Celanovic, I., Soljacie, M., SELECTIVE SOLAR ABSORBERS. *Annual Review of Heat Transfer* **2012**, *15*, 231–254.
24. Lee A. Weinstein, James Loomis, Bikram Bhatia, David M. Bierman, Evelyn N. Wang, Gang Chen , Concentrating Solar Power. *Chemical Reviews* **2015**, *115*.
25. Almeco Group. https://www.almecogroup.com/
26. Alanod. https://alanod.com/
27. Kennedy, C. E.,Review of Mid- to High-Temperature Solar Selective Absorber Materials, **2002**.
28. N.Selvakumar, Harish C.Barshilia , Review of physical vapor deposited (PVD) spectrally selective coatings for mid- and high-temperature solar thermal applications. *Solar Energy Materials and Solar Cells* **2012**, *98*, 1–23.
29. Yang, D., Zhao, X., Liu, Y., Li, J., Liu, H., Hu, X., Li, Z., Zhang, J., Guo, J., Chen, Y., Yang, B. ,Enhanced thermal stability of solar selective absorber based on nano-multilayered AlCrSiO films. *Solar Energy Materials and Solar Cells* **2020**, *207*.
30. Benz, N., Beikircher, T. , High efficiency evacuated flat-plate Solar Collector for process steam production. *Solar Energy* **1999**, *65*, 111–118.
31. TVP Solar. https://www.tvpsolar.com/
32. Buonomano, A., Calise, F., d'Accadia, M. D., Ferruzzi, G., Frascogna, S., Palombo, A., Russo, R., Scarpellino, M. , Experimental analysis and dynamic simulation of a novel high-temperature solar cooling system. *Energy Conversion and Management* **2016**, *109*, 19–39.
33. Moss, R. W., Henshall, P., Arya, F., Shire, G. S. F., Eames, P. C., Hyde, T. , Simulator testing of evacuated flat plate solar collectors for industrial heat and building integration. *Solar Energy* **2018**, *164*, 109–118.

34. Moss, R. W., Henshall, P., Arya, F., Shire, G. S. F., Hyde, T., Eames, P. C. , Performance and operational effectiveness of evacuated flat plate solar collectors compared with conventional thermal, PVT and PV panels. *Applied Energy* **2018**, *216*, 588–601.
35. Li, X.-F., Chen, Y.-R., Miao, J., Zhou, P., Zheng, Y.-X., Chen, L.-Y., Lee, Y.-P. , High solar absorption of a multilayered thin film structure. *Optics Express* **2007**, *15*.
36. Zhou, W.-X., Shen, Y., Hu, E.-T., Zhao, Y., Sheng, M.-Y., Zheng, Y.-X., Wang, S.-Y., Lee, Y.-P., Wang, C.-Z., Lynch, D. W., Chen, L.-Y. , Nano-Cr-film-based solar selective absorber with high photo-thermal conversion efficiency and good thermal stability. *Optics Express* **2012**, *20*.
37. David L. Windt , IMD—Software for modeling the optical properties of multilayer films. *American Institute of Physics*. **1998**.
38. Russo Roberto, Monti M., Di Giamberardino F., Palmieri V. G., Characterization of selective solar absorber under high vacuum. *Optics Express* **2018**, *26*.
39. Carmine D'Alessandro, Davide de Maio, Daniela de Luca, Emiliano di Gennaro, Mariano Gioffrè, Mario Iodice, Marilena Musto, Giuseppe Rotondo, Davide Dalena, Roberto Russo , Solar Selective Coating for Thermal Applications. *Key Engineering Materials* **2019**, *813*, 316–321.
40. H. Watanabe, M. Susa, H. Fukuyama, K. Nagata, Near-Infrared Spectral Emissivity of Cu, Ag, and Au in the Liquid and Solid States at Their Melting Points. *International Journal of Thermophysics* **2003**, *24*.
41. R. Smalley, A. J. Sievers , The total hemispherical emissivity of copper. *Journal of the Optical Society of America* **1978**, *68*.
42. Xu, K., Hao, L., Du, M., Mi, J., Yu, Q., Li, S., Wang, J., Li, S. , Thermal emittance of Ag films deposited by magnetron sputtering. *Vacuum* **2020**, *174*.